

Seasonal patterns of near-bottom chlorophyll fluorescence in the eastern Chukchi Sea: 2010–2019

Phyllis J. Stabeno^{a,*}, Calvin W. Mordy^{a,b}, Michael F. Sigler^c

^a NOAA Pacific Marine Environmental Laboratory, 7600 Sand Point Way NE, Seattle, WA, 98115-0070, USA

^b University of Washington, JISAO, 7600 Sand Point Way NE, Seattle, WA, 98115-0070, USA

^c NOAA Alaska Fisheries Science Center, Retired, 17109 Point Lena Loop Road, Juneau, AK, 99801-8344, USA

ARTICLE INFO

Keywords:

Chukchi Sea
Sea ice
Fluorescence
Ice algae

ABSTRACT

The Chukchi Sea consists of a broad, shallow (<45 m) shelf that is seasonally (November–July) covered by sea ice. This study characterizes the seasonal patterns of near-bottom primary production using moored instruments measuring chlorophyll fluorescence, oxygen, nitrate, and photosynthetically active radiation. From 2010 to 2018, moorings were deployed at multiple sites each year. Instruments were restricted to within 10 m of the seafloor due to ice keels, which can reach 30 m below the surface in this region. Near-bottom blooms were common at all mooring sites. The bloom onset directly followed ice retreat whereas the end of the bloom followed loss of light in September. The intensity of light at the seafloor (~40 m deep) was similar to levels observed under 1–2 m thick ice floes in the spring/early summer, and was sufficient to support photosynthesis near the seafloor, utilizing nitrate and producing oxygen. We hypothesize that the near bottom bloom originated from aggregates of ice algae that sank during ice retreat. As a consequence of climate warming and earlier ice retreat, we predict that the near-bottom bloom onset will occur earlier, but the timing of the end of the near-bottom bloom will remain the same pending a sufficient nutrient supply. The Chukchi Sea is highly productive even though the growing season is short. This production is promoted by a shallow seafloor, which allows multiple production layers (surface open water, bottom of the mixed layer, under-ice algae, and disassociated ice algae which settles near the seafloor). We term this the Multiple Production Layers (MPL) hypothesis.

1. Introduction

The Chukchi Sea consists of a broad shallow shelf, extending >800 km northward from the Bering Strait to the shelf break and the Arctic basin. It is characterized as an inflow shelf for the Arctic (Carmack and Wassmann, 2006) and is the sole source of Pacific water to the Arctic Ocean. The flow through Bering Strait provides heat, freshwater, and salt, including nutrients, to the Chukchi Sea and the Arctic Basin. The northward flow divides into two primary branches — the western branch flows into the Arctic basin through Herald Canyon and the eastern branch flows through Barrow Canyon (Coachman et al., 1975).

Sea-ice algae are a major source of carbon to the benthic ecosystem (Grebmeier, 2012; Koch et al., 2020) with an estimated production during spring of 1–2 g C m⁻² (Gradinger, 2009). Production of ice algae is primarily limited by light (Michel et al., 1988; Welch and Bergmann, 1989) and nutrients (Cota et al., 1987; Castellani et al., 2017).

The spring plankton bloom likely initiates under and within the sea

ice (Hill and Cota, 2005; Arrigo et al., 2012; Lowry et al., 2018; Tedesco et al., 2019). Seasonal ice retreat favors the export of aggregates of under-ice algae directly to the benthos (Ambrose et al., 2005; Boetius et al., 2013; Katlein et al., 2015; Koch et al., 2020). This, together with benthic microalgae, support the Chukchi's rich, benthic-dominated ecosystem (Dunton et al., 2014).

There has been a dramatic loss of sea ice in the Chukchi Sea during the last 15 years (Wood et al., 2015, 2018; Serreze et al., 2016; Frey et al., 2015), with earlier ice retreat in the spring/summer and later ice arrival in the fall. This loss of sea ice (including multi-year ice) has increased the atmospheric heat-flux into the Chukchi Sea (Danielson et al., 2020). Earlier ice retreat also impacts the timing of export of ice algae to the seafloor and the timing of open water phytoplankton production (Arrigo et al., 2008; Hill et al., 2017), and favors open water phytoplankton primary production that benefits a pelagic ecosystem (Grebmeier et al., 2006, 2015; Moore and Stabeno, 2015). A longer open-water season is predicted to alter the composition and distribution

* Corresponding author.

E-mail address: phyllis.stabeno@noaa.gov (P.J. Stabeno).



of phytoplankton communities (Tremblay et al., 2009; Neeley et al., 2018).

The focus in this paper is to examine the relationship among chlorophyll fluorescence, arrival and departure of sea ice, and photosynthetically active radiation (PAR). We utilize a variety of data sources, including hydrographic casts, pop-up buoys (a newly developed technology that measures properties underneath the ice), and a variety of time series collected on moorings. Chlorophyll fluorescence, PAR, oxygen, and nitrate were measured near the seafloor at multiple mooring sites on the U.S. Chukchi Shelf over a 9-year period (Fig. 1). These instruments were all deployed within 8 m of the seafloor to avoid the deep ice keels that can occur on this shelf.

Preliminary analysis indicated that the large export of ice algae to the seafloor coincides with ice retreat (Berchok et al., 2015). In their analysis, an increase in percent oxygen saturation and/or decrease in nitrate concentration were often associated with this export event, suggesting that net primary production due to ice algae continues at depth. We contend that this continued production is not due to subsurface phytoplankton, which lie shallower, but rather near-bottom disassociated ice algae. We present evidence to support this distinction in the results and discussion.

Our objective was to test the multiple production layer or MPL, ‘maple’, hypothesis that ice algae fall to the seafloor as ice retreats and continue to photosynthesize for weeks or longer (Fig. 2). According to this hypothesis, this near-bottom layer of continued photosynthesis by disassociated ice algae adds to the other layers of primary production (i.e. sympagic algal production, and surface and sub-surface phytoplankton blooms) that together account for the high primary productivity found on the Chukchi Shelf (Hill and Cota, 2005; Arrigo et al., 2012; Codispoti et al., 2013; Hill et al., 2017).

2. Data and methods

2.1. Moorings

Moorings (Fig. 1) were deployed at 8 sites (C1–C8) on the Chukchi Shelf during late summer and recovered the following summer, when new moorings were usually deployed. Listed in Table 1 are the deployment years at each site, mooring locations and instrumentation. All moorings were short, taut wire moorings. During winter and spring, sea-ice keels can be as deep as 30 m below the surface (Stabeno et al., 2018). To avoid these ice keels, each mooring was <10 m tall, keeping the upper float at least 30 m below the surface. This height limitation

resulted in two moorings being deployed at each site, because of the limited amount of vertical wire space. Instruments on the moorings collected hourly measurements of the following variables: temperature (SeaBird SBE-37, SBE-39, SeaCat); currents (Acoustic Doppler Current Profiler, RCM-9); salinity (SBE-37, SeaCat); chlorophyll fluorescence (Sea-Bird/WET Labs FLSB ECO Fluorometer); nitrate (Sea-Bird/Satlantic ISUS or SUNA; at selected sites); and PAR (Biospherical Instruments QSP2300). Excluding the ADCP that was deployed at the top of the mooring, the rest of the instruments were deployed 4–8 m above the bottom. All instruments were prepared according to manufacturers’ specifications and calibrated prior to deployment (except for calibration of the nitrate sensors which is discussed below). While chlorophyll samples were taken at the mooring sites on deployment and recovery of the moorings, there were insufficient data to improve the conversion of fluorescence to chlorophyll.

To reduce biofouling, optical wipers on the Eco Fluorometer and SUNA were engaged prior to each hourly set of measurements, and the ISUS sensors were plumbed into the outflow of a Sea-Bird Scientific SBE-16 with anti-fouling agents mounted on either side of the ISUS flow cell. See Mordy et al. 2020 for further details of data processing of nitrate sensors.

2.2. Hydrography

The conductivity-temperature-depth (CTD) instrument package consisted of a Sea-Bird 911plus with dual sensors measuring temperature, conductivity and oxygen, and single sensors measuring, pressure, and chlorophyll fluorescence. Hydrographic casts were done at each mooring site upon deployment and/or recovery of moorings. While the optical nitrate sensors (ISUS and SUNA) have a reported accuracy of ~2 μM , they must be calibrated with discrete samples. At the depth of the nitrate sensor, discrete samples for nutrients were collected from Niskin bottles and filtered through 0.45 μm cellulose acetate filters. Samples were frozen for analysis at our laboratory in Seattle, WA. See Mordy et al. 2020 for details of the analysis.

On July 18, 2015, aboard the USCGC Healy cruise HE1501, a GoPro camera was attached to the top of the CTD frame and a movie was taken simultaneously with the CTD downcast near the C2 mooring (164.3°W, 71.2°N). Three representative frames were selected from this movie and presented herein, and a short video segment is included in the supplemental material (Supplemental Video).

2.3. Pop-up buoy

During the last four years, pop-up buoys have been developed at the Pacific Marine Environmental Laboratory (Langis et al., 2018). The purpose of this effort was to develop an inexpensive, expendable buoy to make under-ice measurements that could be deployed in summer or fall and rise to the surface in the following winter or spring on a prearranged day. Eventually, when the ice melted, the buoy surfaced and transmitted data back to the laboratory. The instruments collect data during three unique periods: (1) on the seafloor; (2) on the vertical profile as it rises to the surface; and (3) under the ice.

The buoy presented in this manuscript is Generation 3. It consisted of a spherical float (30 cm in diameter). The upper ~5 cm of top had been cut off, and a flat plate (cap) attached at the top. One thermistor ($\pm 0.01^\circ\text{C}$) was located on the top-cap and a second one at the bottom of the float. A fluorometer ($\pm 2\%$) was located on the bottom of the float facing downwards, while the PAR sensor ($\pm 3\%$) and pressure sensor ($\pm 0.21 \text{ m}$) were located on the top-cap. The camera (UCAM III Low-Resolution Digital Camera) was tilted upward at 45° and positioned ~10 cm from the bottom of the ice.

2.4. Sea ice

The Advanced Microwave Scanning Radiometer (AMSR-E) data

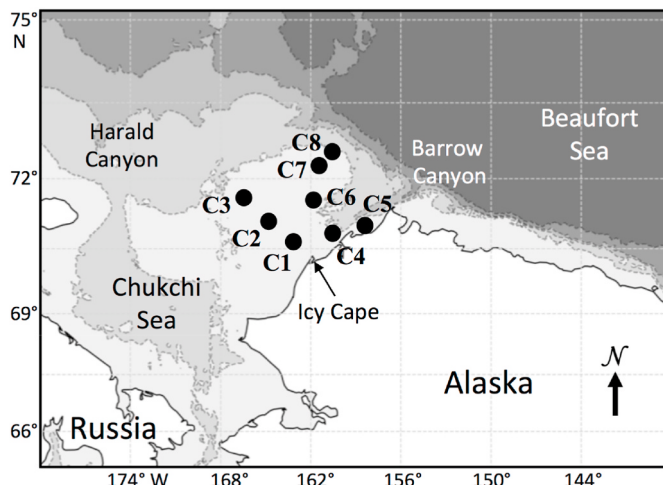


Fig. 1. Map of the Chukchi Sea shelf with bathymetry and place names. The eight shelf mooring sites (C1–C8) are indicated by black dots. The periods of deployments are listed in Table 1.

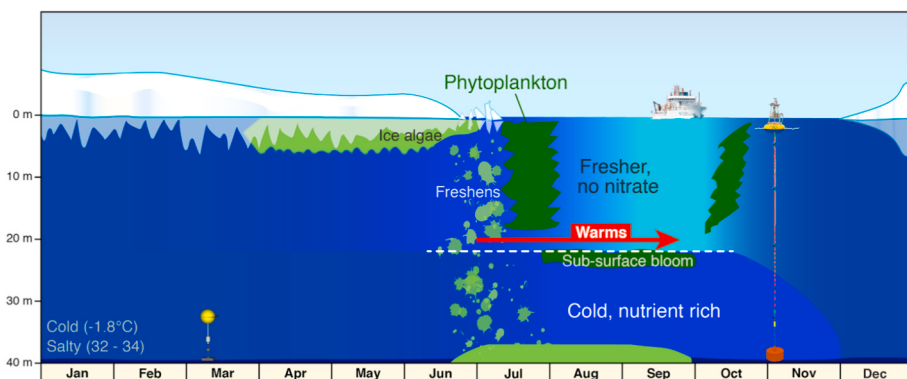


Fig. 2. Seasonality of the lower trophic level of the ecosystem on the northeastern Chukchi Sea Shelf. Ice algae bloom occurs beneath the ice in spring, and with ice melt it is exported to the bottom, where there is sufficient light and nutrients to support further production. With ice retreat/melt the water stabilizes with a relatively warm, low salinity surface layer overlaying a colder, more saline bottom layer. With this stabilization, a surface phytoplankton bloom can occur consuming the remainder of surface nutrients and support a subsurface bloom. With surface mixing in late summer a fall phytoplankton bloom may occur (Adapted from Fig. 136, Berchok et al., 2015).

Table 1

List of moorings (with depth in parentheses) and instruments deployed between 2010 and 2017. F indicates the fluorometer functioned correctly providing data for the entire deployment. Similarly, N is a nitrate sensor, O an oxygen sensor and P a PAR sensor. Bold indicates that the instrument recorded data for only part of the deployment cycle. “Yes” indicates that there was production in the near bottom; “No” indicates that there was no production; and “-“ indicates that there were insufficient data to decide. In addition to the variables listed below, currents were measured at most sites. The depths of each instrument were 4–8 m above the bottom.

Site (depth)	Lat. Long.	Aug 2010	Aug 2011	Aug 2012	Aug 2013	Sep 2014	Sep 2015	Aug 2016	Aug 2017
C1 (45 m)	70.835 163.119	FNOP yes	FO -		FNOP -	NP -	FNOP yes	FNOP yes	FNP yes
C2 (44 m)	71.222 164.250	FNOP yes	FNOP yes	FOP yes	FOP yes	FNOP yes	FNOP yes	FNOP yes	FNOP yes
C3 (45 m)	71.825 165.975	OP -	FNO yes					NP -	FNOP yes
C4 (48 m)	71.042 160.493			OP -	FOP -	FNP yes	FOP yes	FP -	FOP yes
C5 (45 m)	71.207 157.999				FON yes	FNOP yes		FP -	FP -
C6 (43 m)	71.777 161.875				FN no	FN -			
C7 (43 m)	72.424 161.604				FN yes	FN yes			
C8 (46 m)	72.586 161.215					FO yes			

(available from the National Snow and ice Data Center, <http://nsidc.org/data/amsre/>) were used in this manuscript. AMSR is a dataset of sea-ice extent and areal concentration consisting of daily ice concentration data at 12.5 km resolution. Time series of percent areal coverage were calculated in 50 km × 50 km boxes around each mooring site (C1–C8).

2.5. Data analysis

Time series of sea-ice coverage (percent) values were used to determine the timing and duration of the ice-free period in summer. These records were plotted, and the retreat and return dates were assigned (Table S1, Fig. S1). Ice retreat was considered to have occurred when areal sea-ice cover fell below 15% for the first time during each year. Ice return was considered to have occurred when areal ice cover increased above 15% for the last time during each year. The duration of the ice-free period was computed as the difference in days between ice retreat and ice return.

PAR values near the seafloor for each mooring and year were examined to determine the time and duration of the photic period in summer. These records were plotted and the onset, end and maximum

value of PAR were assigned (Table S1, Fig. S1). Onset and end of the PAR period were considered to have occurred when the PAR value crossed a threshold of $0.1 \mu\text{E m}^{-2} \text{s}^{-1}$ (Hancke et al., 2018). PAR duration was computed as the difference in days between PAR end and PAR onset.

Chlorophyll values near the seafloor for each mooring and year were examined to determine the time and duration of the bloom in summer (herein we use “bloom” to indicate increased chlorophyll fluorescence). These records were plotted and the onset, end and maximum value of the summer bloom were assigned (Table S1, Fig. S1). Onset and end of the near-seafloor summer bloom (“bloom end”) were considered to have occurred when the concentration of chlorophyll crossed $1 \mu\text{g l}^{-1}$ (Arigo and van Dijken, 2011). Bloom duration was computed as the difference in days between bloom end and bloom onset.

Annual values of ice retreat, ice return, PAR onset, PAR end, bloom onset, and bloom end were plotted by year and mooring using box plots and the R package ‘ggplot2’. The relationships between values (e.g. between bloom onset and ice retreat) were plotted by year and mooring using the R package ‘ggplot2’ scatter plots. Their relatedness was examined by computing Pearson correlation coefficients r (e.g., between bloom onset and ice retreat) and the statistical significance of the r -values were estimated using the R package ‘Hmisc’.

3. Results

3.1. Sea ice

Typically, ice cover was at or near 100% during winter for most mooring sites (Fig. 3a, Fig. S1). The exceptions were the three most coastal moorings—primarily C4 and C5 and, to a lesser extent, C1. At these sites, winter and spring sea-ice cover was usually reduced when strong winds were out of the east and/or northeast (referred to as a wind-driven polynya) or when warm Atlantic water surfaced (referred to as a sensible heat polynya) (Ladd et al., 2016; Hirano et al., 2016). At these coastal moorings, areal ice concentration during winter was smallest in 2013, 2014, and 2016 (Fig. 3a). The greatest variability in areal ice cover was at C4 and C5, the two moorings nearest the shelf break (Figs. 1 and 3b). At all the mooring sites discussed herein, sea ice eventually retreated in summer, and returned in late summer or fall (Fig. S1).

The timing of sea-ice retreat varied among years with later retreats in 2012–2014 and earlier retreats in 2010–2011 and 2015–2017 (Fig. 4a). The median day of ice retreat was approximately day 170 (mid-June) for 2010–2011, day 205 (late July) for 2012–2014, day 190 (early July) for 2015–2016, and day 135 (mid-May) for 2017. This pattern of two years of early retreat, three of late, two of mid-range, and finally one year of early ice retreat largely occurred regardless of location, with some exceptions. For example, ice retreat at C7 and C8 in 2010 was similar to the later ice retreat observed in 2012–2014. At C4, the early ice retreat in 2012 reflects a brief period of low ice followed by a return of sea ice lasting several weeks (Fig. S1).

The timing of sea-ice return varied less than sea-ice retreat, with most returns occurring between days 300 and 330 (November; Fig. 4d). The range of sea-ice return was much narrower (~50 days, day 294–345) than the range of sea-ice retreat (~100 days, day 133–232) (Table S1). Thus, variability in the duration of the ice-free period was dictated more by ice retreat than ice return and ranged from 67 to 203 days. The median duration of the ice-free period was 127 days.

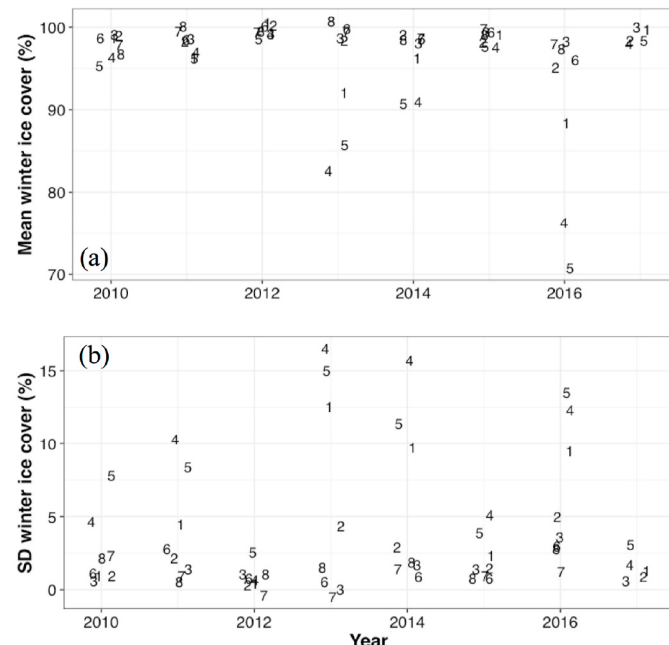


Fig. 3. (a) The mean winter (January–March) ice cover at each mooring site as a function of year. (b) The standard deviation of the mean winter ice cover shown in (a). The individual moorings are indicated by number, so “4” refers to the mooring site C4. The points are randomly offset to reduce overlap. The coastal moorings C1, C4, and C5 had periods of low ice cover and the greatest variability.

3.2. Ice algae

3.2.1. Under-ice data from pop-up buoy

An under-ice (water-ice interface) bloom was observed during spring 2019 from a pop-up buoy that floated to the surface and came to rest at the bottom of an ice floe for approximately two months (May and June). The pop-up buoy was deployed in August 2018 near the C2 mooring (71.2°N, 164.3°W). It remained anchored to the sea floor until April 30, 2019, when the pop-up buoy was released (as designed) and rose to the surface underneath a large (~20 km long) ice floe (Fig. 5a). This distinctive floe was tracked via satellite images until 20 June, when the ice floe began to break apart. The floe traveled a distance of ~400 km over a period of 60 days (blue line, Fig. 5b). During this period, the pop-up buoy successfully collected hourly temperature, PAR and fluorescence data just below the bottom of the ice. The top of the buoy rested immediately below the ice at a depth of ~1.5 m (an indication of ice thickness) during the first ~25 days and then began to shoal (an indication of ice thinning) (Fig. 5c).

Chlorophyll fluorescence near the ice-seawater interface began to increase on ~14 May and the bloom continued through early June (Fig. 5d). This bloom occurred under low light conditions (max 2–3 $\mu\text{E m}^{-2} \text{s}^{-1}$ prior to 27 May); PAR increased reaching 4–8 $\mu\text{E m}^{-2} \text{s}^{-1}$ in early June. In mid-June, the fluorescence disappeared and PAR increased to 20 $\mu\text{E m}^{-2} \text{s}^{-1}$. It was unlikely that the disappearance of the bloom was related to photoinhibition because Cota and Horne (1989) found that, even for ice algae adapted to low light, photo inhibition does not occur until ~40 $\mu\text{E m}^{-2} \text{s}^{-1}$. While nutrient depletion and grazing cannot be discounted, the expectation is that the bloom sank toward the sea floor once the ice substrate began to erode (Fig. 5c), which is consistent with loss of color in the under-ice images (Fig. 5f and g) (Riebesell et al., 1991; Ambrose et al., 2005; Boetius et al., 2013; Fernández-Méndez et al., 2014; Katlein et al., 2015).

The pop-up buoy remained in the vicinity of moorings C2 and C3 for ~25 days (Fig. 5b). This provided simultaneous time series of fluorescence underneath the ice and near the seafloor (Fig. 6). While in the vicinity of C2 (red line Fig. 6a), the under-ice chlorophyll fluorescence was near-zero as was the near-bottom chlorophyll fluorescence. As the buoy came closer to C3, under-ice fluorescence began to increase (green line). The near bottom fluorescence began to increase at C3 ~20 days after it began to increase at the ice-water interface (green line in Fig. 6b). This lag is consistent with estimates of settling rates of ice algae (0.4–2.7 m d^{-1} , Michel et al., 1993).

3.2.2. Water column data from CTD and video

Vertically, there can be multiple layers of significant chlorophyll fluorescence in the Chukchi Sea (Martini et al., 2016). This multilayer pattern was evident in a hydrographic cast done in 2015 (Fig. 7, left), when a camera was attached to the CTD frame (photos in Fig. 7, right). This CTD cast (164.3°W, 71.2°N on July 18, 2015) was taken near C2, approximately 3 days after the ice retreated. Two increases in chlorophyll fluorescence are evident in the cast data, a relatively small one at ~15 m and a larger one below 20 m. The photos show the different quality of the blooms. The photo of the upper water column appears fairly clear (Fig. 7, photo A); the middle photo shows a diffuse chlorophyll peak and likely represents a subsurface phytoplankton bloom associated with the pycnocline (Fig. 7, photo B), while the bottom photo (Fig. 7, photo C) has larger aggregates of cells and extends over ~10 m depth (Fig. 7, left). As the CTD passed the halfway point through the lower layer of fluorescence (~28 m), PAR was fully attenuated. These aggregates are better viewed and clearly visible by video (Supplementary Video), and consistent with reports of sinking aggregates of disassociated ice algae (Riebesell et al., 1991; Ambrose et al., 2005; Boetius et al., 2013; Fernández-Méndez et al., 2014; Katlein et al., 2015; Koch et al., 2020).

Identifying these aggregates as disassociated ice algae at our moorings is supported by observations at a nearby sediment trap deployed on

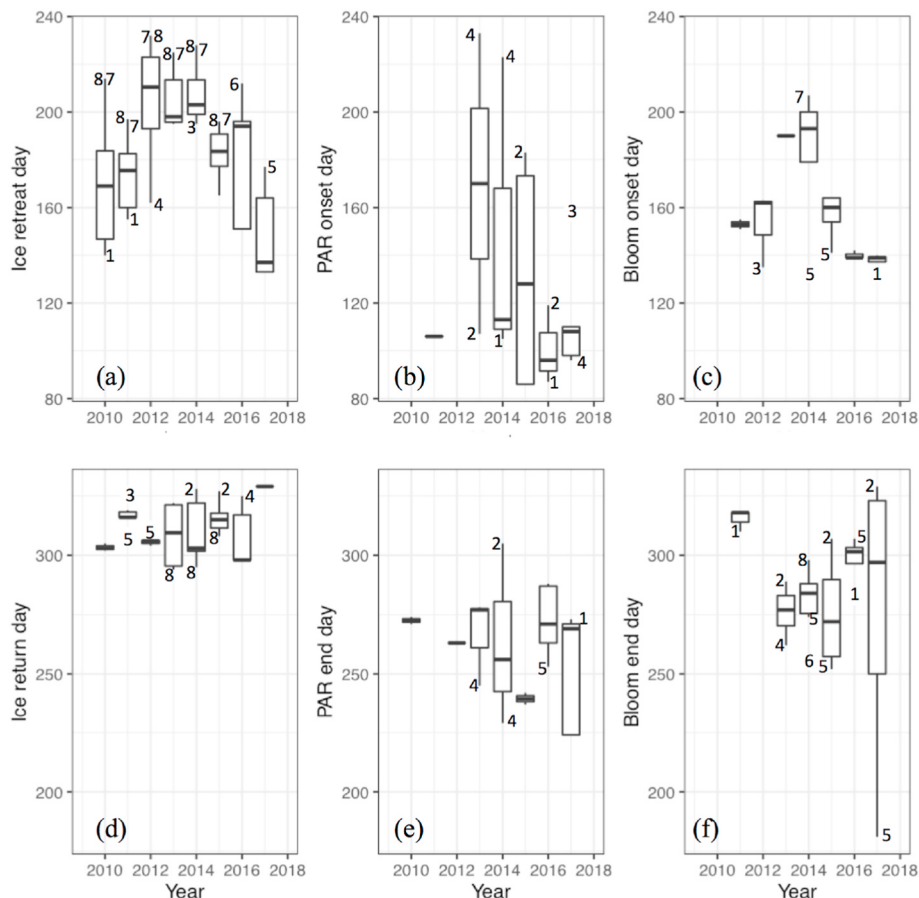


Fig. 4. Box plots indicating (a) day of ice-retreat, (b) day on which the onset of $\text{PAR} > 0.1 \mu\text{E m}^{-2} \text{s}^{-1}$, (c) day of bloom onset, (d) day of ice-return, (e) day on which PAR falls below $0.1 \mu\text{E m}^{-2} \text{s}^{-1}$, and (f) day of bloom end day, all versus year of mooring deployment. The data shown herein are from S1. The numbers in each panel indicate the mooring sites (e.g. "4" refers to C4) that are outside the interquartile range.

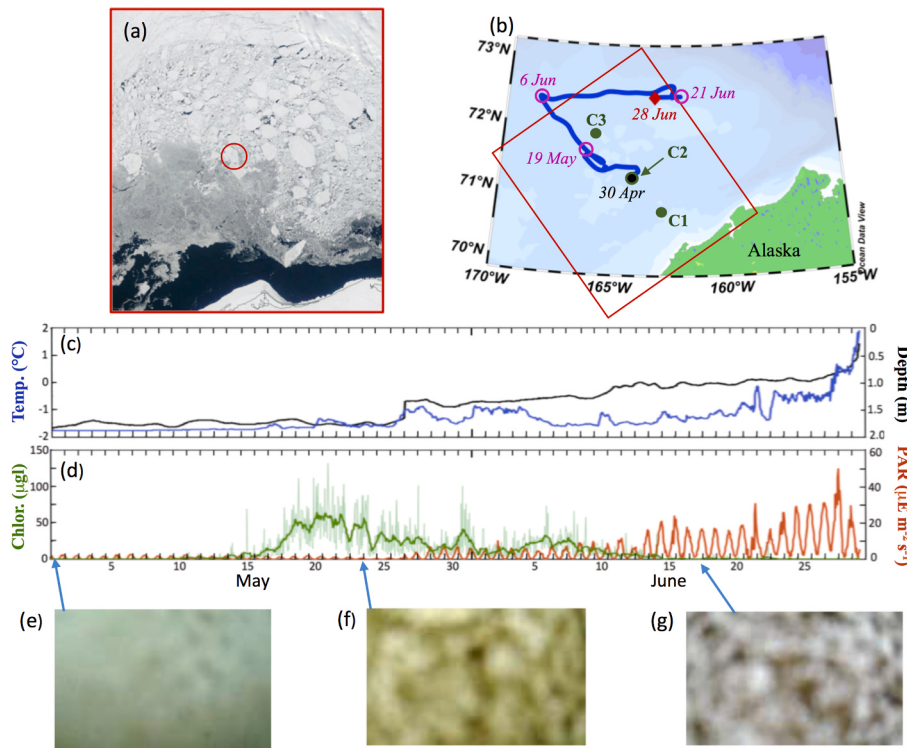


Fig. 5. (a) Satellite image of sea ice on April 30, 2019 when the pop-up buoy surfaced. The red circle indicates the location of where the pop-up buoy was deployed. (b) The trajectory of the ice floe from 30 April to 28 June when it broke apart and the buoy began to transmit location and data (red dot). Selected dates are indicated in purple. Mooring locations are shown and color-coded. The red box is the area shown in (a). (c) Time series of temperature beneath the sea ice and the depth of buoy. The depth of buoy is effectively the thickness of the sea ice at that point because the buoy sits immediately beneath the ice. (d) Time series of chlorophyll fluorescence and PAR measured below the ice by instruments on the pop-up buoy. (e-g) Photos of the water column. (For interpretation of the references to color in this figure legend, the reader is referred to the Web version of this article.)

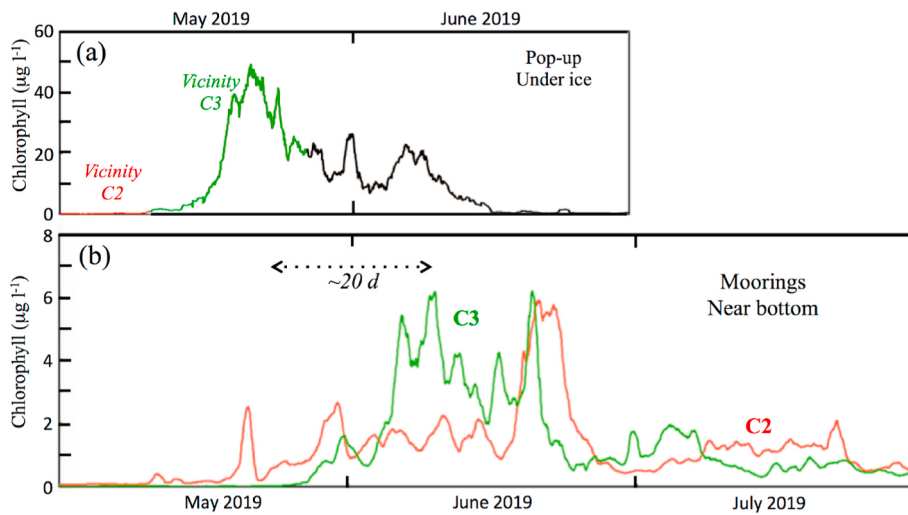


Fig. 6. (a) Low-pass filtered time series of chlorophyll fluorescence measured by pop-up buoy under the ice. It is color coded with red indicating when the buoy was in the vicinity of C2, green in the vicinity of C3, and black in the vicinity of no mooring. (b) Low-pass filtered time series of near-bottom chlorophyll fluorescence measured at C2 (red) and C3 (green). (For interpretation of the references to color in this figure legend, the reader is referred to the Web version of this article.)

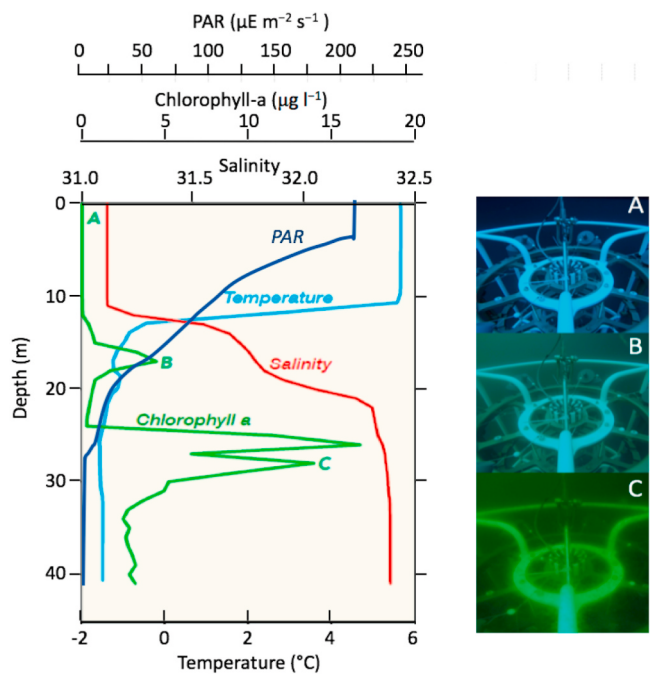


Fig. 7. (left) Hydrographic cast in 2015 near C2 showing multiple subsurface chlorophyll maxima. A smaller subsurface maximum was observed just below the pycnocline, and a larger maximum was observed in the bottom layer. (right) Photos of the water column (taken from a video in the supplemental material): upper layer of relatively clear water; first chlorophyll maximum below the pycnocline; and at the top of the large maximum. The letters A, B, and C correspond to the appropriate depth shown on the left.

the northern Chukchi Shelf in 2016 (Koch et al., 2020). Koch et al. (2020) found that as ice retreated, the flux of sea-ice exclusive diatoms (*Nitzschia frigida* and *Melosira arctica*) increased from ~ 2 million cells $m^{-2} d^{-1}$ in early June to ~ 30 million cells $m^{-2} d^{-1}$ in early July. This was accompanied by a 10-fold increase in the flux of lipids that are specific to sympagic organisms (from ~ 100 to 1000 ng $m^{-2} d^{-1}$). The timing of this flux was concurrent with the increased concentrations of chlorophyll observed at two nearby moorings, C2 (60 km away) and C4 (80 km) (Fig. S1).

3.2.3. Near-bottom data from mooring C2 in 2018

The fate of these sinking aggregates can be seen in the time series (oxygen, nitrate, PAR and fluorescence) collected at the moorings. For example, in 2018 at mooring C2, the ice retreated in mid-May (Fig. 8a), an early date for ice retreat, and there was a sharp increase in chlorophyll fluorescence in the near-bottom water (30–40 m below the surface; Fig. 8b). Accompanying this increase in fluorescence was a sharp increase in the percent saturation of oxygen, from $\sim 90\%$ to $>120\%$, and, at the same time, a decrease in nitrate from $\sim 15 \mu M$ to near $0 \mu M$

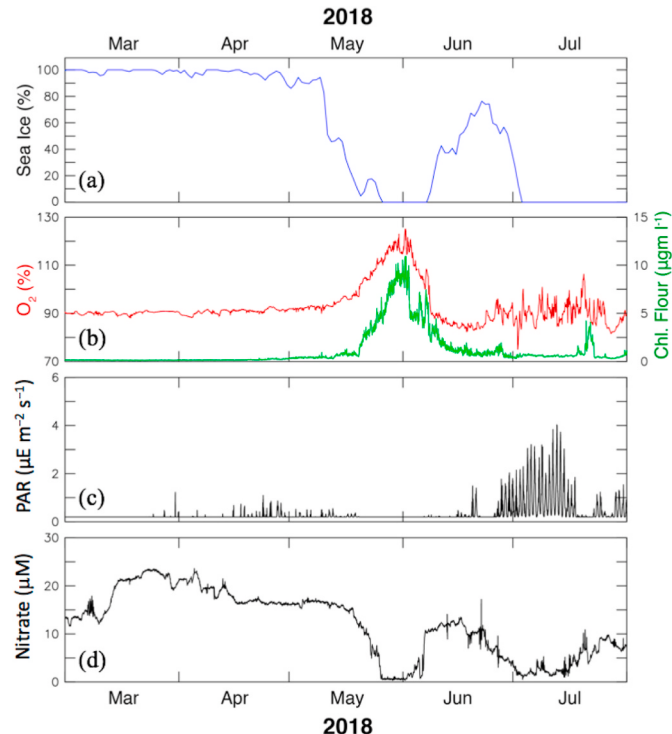


Fig. 8. Time series of: (a) percent ice cover in $50 \text{ km} \times 50 \text{ km}$ box centered on C2; (b) percent oxygen saturation (red) and chlorophyll fluorescence (green); (c) PAR; and (d) nitrate. Except for (a), all time series were measured on mooring at C2 within 8 m of the bottom. (For interpretation of the references to color in this figure legend, the reader is referred to the Web version of this article.)

(Fig. 8d) consistent with active photosynthesis in the bottom waters. Light (PAR) was very weak ($<2 \mu\text{E m}^{-2} \text{s}^{-1}$), but measurable through mid-May, decreasing to near zero during the period of high chlorophyll fluorescence; it increased markedly in early July with the disappearance of fluorescence. We suspect that the decrease in PAR to near zero in mid-May was a result of disassociated ice algae descending as a mass through the water column, and the resulting shading prevented most of the light from reaching the seafloor. Such a shading (sharp decrease in PAR) effect was also evident in Fig. 7a, when the CTD entered the region with high chlorophyll. The highest PAR values (Fig. 8c) occurred in July when near-bottom chlorophyll concentrations were low and ice was absent. Vertical mixing in the bottom ~ 8 m during late May - early June likely exposes the ice algae to sufficient light to continue production; that is, sometimes cells are at the top of the layer and exposed to sufficient light and then mixed downward in this bottom mixed layer.

Near the seafloor, chlorophyll fluorescence began decreasing between 1–6 June, perhaps due to nutrient limitation or grazing (Fig. 8b, d). On 7 June, sea ice returned, and there was a sharp increase in nitrate, and reductions in chlorophyll fluorescence and oxygen saturation ($<90\%$), results consistent with advection of water past the mooring (Mordy et al., 2020) and net respiration. When the ice retreated for the second time in early July, the highest PAR was recorded and yet there was no clear evidence of active photosynthesis as chlorophyll fluorescence remained low and oxygen saturation, while variable, was $<100\%$. Finally, in mid-July there was a small pulse of chlorophyll fluorescence that once again shaded near-bottom waters (low PAR), was coincident with a 5 μM drop in nitrate, and resulted in a short period of $>100\%$ oxygen saturation.

3.3. Near-bottom chlorophyll and its relationship to sea ice and light level

Continued fluorescence and photosynthesis near the seafloor following ice retreat was common in our time series. This pattern (described in the previous section for mooring C2 in 2018) of ice retreat, increased fluorescence, increased oxygen (by $>20\%$) and/or decreased nitrate dominates at the mooring sites over the years (2010–2018), occurring 22 out of 23 times (96%) when there are sufficient data to detect this pattern (Table 1). Each of these locations is shallow (<48 m) with measurable light (PAR) reaching the bottom. In MPL, we have hypothesized that the increased fluorescence was likely due to continued photosynthesis by disassociated ice algae near the seafloor, as evidenced by accumulation of sea-ice exclusive diatoms in a sediment trap (Koch et al., 2020) and increasing percent oxygen saturation and/or decreasing nutrients (Fig. 8). In the next few paragraphs, we explore the relationship among the timing and duration of the chlorophyll fluorescence bloom, ice retreat and duration, and the magnitude of PAR.

The timing of PAR onset ($>0.1 \mu\text{E m}^{-2} \text{s}^{-1}$) was earlier for 2011, variable and often later for 2013–2015, and earlier for 2016–2017 (Fig. 4b). The median of PAR onset was approximately days 95–130 for all years except in 2013, when the median was about day 170. Unlike the timing of PAR onset, the timing of PAR end was similar regardless of the year. In general, the range of PAR end (~ 80 days, day 224–305) was much narrower than the range of PAR onset (~ 150 days, day 86–233) (Supplemental Table S1). Thus, the duration of the PAR period was dictated more by the timing of PAR onset than the timing of PAR end, ranging from 6 (C4 in 2014) to 200 days. The median duration of the PAR period was 151 days (Table S1).

The timing of the algal bloom onset was earlier for 2011–2012, later for 2013–2014, and earlier for 2015–2017 (Fig. 4c). The median day of bloom onset was approximately day 160 for 2011–2012, 190 for 2013–2014, and 150 for 2015–2017. The timing of bloom end was later for 2011, earlier for 2013–2015, and mid-range for 2016–2017 (Fig. 4f). The median day of the end of the bloom was about day 320 for 2011, 280 for 2013–2015, and 300 for 2016–2017. The median duration of the bloom was 128 days and the range was 41–190 days (Table S1). One unusual observation was mooring C5 in 2014, which had a much earlier

bloom onset (approximately day 130) than that year's median (approximately day 190). This bloom began during a period of variable ice cover, but the ice was not so reduced that it reached the 15% threshold that defined ice retreat (Fig. S1).

Comparing the timing of ice, light and the bloom provides evidence that the near-bottom bloom onset occurs at, or prior to, ice retreat, whereas the end of the bloom followed the loss of light in September (Fig. 9). The timing of bloom onset was related to ice retreat ($r = 0.54$, $p = 0.007$) and weakly related to PAR onset ($r = 0.51$, $p = 0.065$) (Fig. 9). The timing of bloom end was weakly related to PAR end ($r = 0.46$, $p = 0.098$) and unrelated to ice return ($r = 0.26$, $p = 0.199$) (Fig. 9). Based on these results, we computed an alternate index of the growing period, the interval between ice retreat and PAR end. We termed this interval the ice retreat-PAR end duration and found that bloom duration is strongly related to ice retreat-PAR end duration ($r = 0.72$, $p = 0.013$) (Fig. 10).

3.4. Annual fluorescence variation during summer

The growing season near the seafloor typically began with the following sequence: ice retreat, a slight increase in PAR, followed by a reduction of PAR concomitant with an increase in near-bottom chlorophyll fluorescence (e.g. Fig. 8). As the ice melted, ice algae were released from the underside of the ice and dropped to the bottom. During the period of the near-bottom bloom (high fluorescence), PAR was particularly low due to self-shading of the bloom. In addition, open-water phytoplankton blooms in the surface layer or below the surface mixed layer (subsurface), common on the northern Chukchi Shelf (Martini et al., 2016), likely contributed to shading of the water column. Another good example of this sequence of events is mooring C2 in 2013 (Fig. S1), where ice cover decreased to 50% in early July and was quickly followed by increased near-bottom chlorophyll concentration. PAR increased concomitant with declining chlorophyll.

As discussed above, sea-ice return did not determine the end of the growing season. Instead the near-bottom bloom was terminated by the seasonal reduction in light during early fall that preceded ice return during our sample years. The usual sequence at the end of the growing season was: PAR becoming undetectable around days 250–270; the near-bottom bloom ending around days 270–300; and ice returning around days 300–320 (Fig. 4).

The near-bottom bloom onset followed directly on ice retreat whereas the end of the bloom followed loss of light in September. As a result, the growing season (bloom duration) near the seafloor was significantly related to the duration of the period between ice retreat and PAR end. In fact, because there was relatively low variability in the ice return day, the PAR end day, and the bloom end day (Fig. 4), the durations of the bloom, PAR, and the ice-free periods were dictated by the timing of their onsets and not their ends.

3.5. Earlier blooms, polynyas and ice-cover variability

Areas of open water during winter and spring occurred in some years. Most often, this happened at mooring sites C1, C4, and C5 (2010, 2011, 2013, 2014, and 2016; Fig. 3). Each of these moorings is near the coast where the Chukchi polynya occurs (Ladd et al., 2016). Intrusion of warmer, saltier Atlantic Water can contribute to or even cause this polynya (Ladd et al., 2016). Earlier blooms were more common in the Chukchi polynya area (C1, C4, and C5) than outside this area. Using the median bloom onset day (day 154) as a threshold to differentiate "early" from "late" bloom onset, 8 of 12 bloom onsets were early in the Chukchi polynya area and only 4 of 12 bloom onsets from this area were late.

Ice retreat is primarily a result of ice melt or of advection forced by local winds and local currents, or a combination of melt and advection (Ladd et al., 2016). The timing of ice retreat (defined here as the first occurrence of areal ice concentration $< 15\%$) varied among the five primary moorings (C1–C5 for the period 2001–2016), with earliest

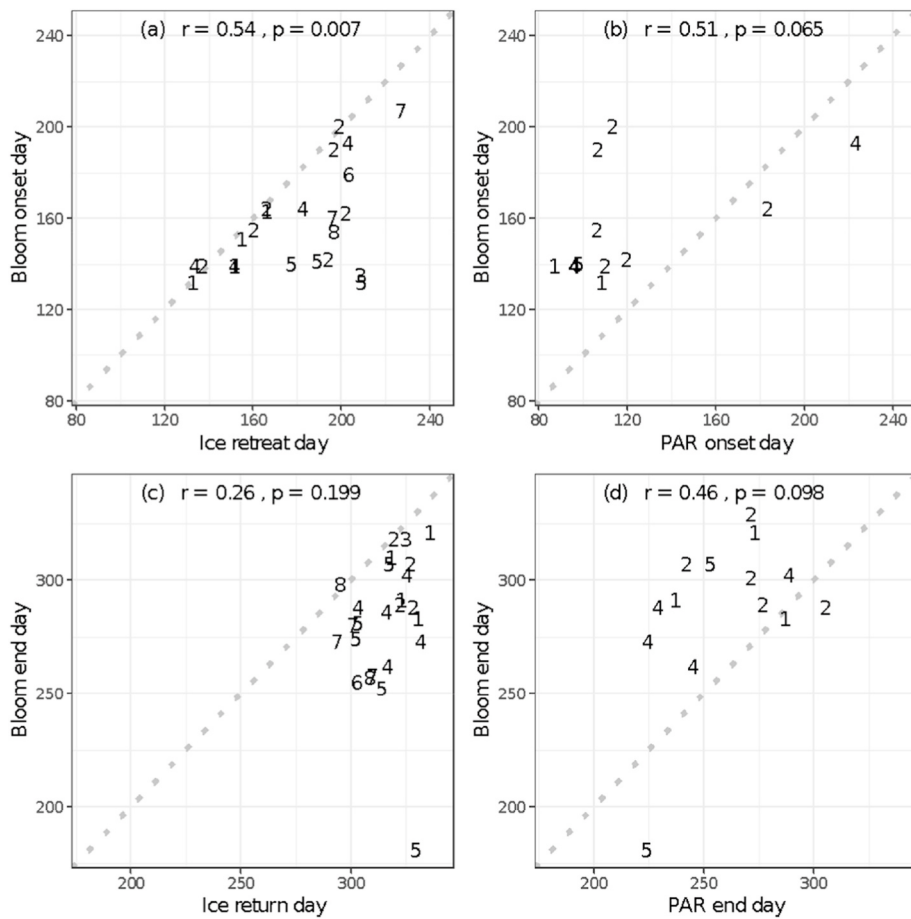


Fig. 9. Scatter plots of the timing of: (a) bloom onset versus ice retreat; (b) bloom onset versus PAR onset; (c) bloom end versus ice return; and (d) bloom end versus PAR end based on near-bottom measurements. The dashed grey line is the 1:1 line.

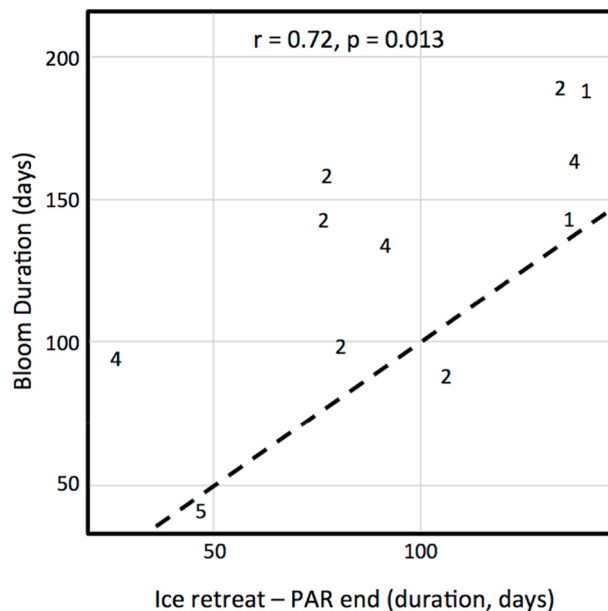


Fig. 10. Scatter plot of the duration of the bloom versus the length of time between ice retreat and PAR end based on near-bottom measurements. The dashed grey line is the 1:1 line.

mean retreat occurring at C1 followed by C4, C2, C3 and, finally, C5. The date of retreat among these five moorings was related with the highest correlation ($r = 0.86$, $p < 0.01$) between the coastal moorings C1 and C4 and the weakest, but still significant, between C1 and C5 ($r = 0.71$, $p < 0.01$). Noting this relationship, the expectation (Fig. 9a) would be that blooms occur earliest at C1 and latest at C3 and C5. Unfortunately, directly examining the timing of the blooms is difficult, because of the limited number of concurrent time series.

Bloom onset was early during years when ice retreated earlier (Fig. 9a) or was episodic in nature. Occasionally ice retreated early, partially returned and then retreated fully for the summer (e.g. mooring C1 in 2012). In this case, a bloom began with the initial ice retreat and continued during the partial return. In other years (e.g. mooring C2 in 2018; Fig. 8) the bloom began with ice retreat and stopped when ice returned. In some years, ice cover was variable during winter and spring (e.g. 2016), PAR increased early (April) and the spring bloom occurred after the early PAR increase (Fig. S1).

Even if ice retreat occurred earlier, an associated chlorophyll maximum was not guaranteed. The earliest observed chlorophyll maxima were during May. For example, a May bloom followed early ice retreat at mooring C5 in 2014 and 2015 (Fig. S1). This can be seen in the 2016 time series; ice cover was irregular in April at moorings C1, C2, and C4, yet substantial fluorescence increases did not occur until May. The lack of a bloom may indicate that either little ice algae were present or the sea ice was advected away (taking its ice algae with it) as opposed to melted.

4. Discussion

4.1. Primary production continues at the seafloor through summer

We found that primary production continued at the seafloor through summer, adding to the primary productivity of the Chukchi Sea, which together with the Chirikov Basin (the region of the northern Bering Sea northeast of St. Lawrence Island) are the most productive regions in the Pacific Arctic (Hill and Cota, 2005; Arrigo et al., 2012; Codispoti et al., 2013; Hill et al., 2017). Virtually all the moorings that successfully measured chlorophyll fluorescence, and either oxygen or nitrate, showed a clear signal of continued production near the seafloor during the summer (Table 1).

We propose that this near-bottom production is due to disassociated ice algae. In most regions with seasonal sea ice, ice algae descend below the photic zone, and thus discontinue to photosynthesize (e.g. Boetius et al., 2013; Rapp et al., 2018). In contrast, much of the Chukchi Sea Shelf is less than 45 m deep and lies within the photic zone. The magnitude of PAR at the Chukchi seafloor was comparable to what was measured beneath the sea ice (Figs. 5d and 8c). Because ice algae can photosynthesize at low levels (Hanche et al., 2018), it is not surprising that photosynthesis by disassociated ice algae may continue near the seafloor. This conclusion is consistent with Koch et al. (2020) who identified disassociated ice algae species together with chlorophyll fluorescence for several months at the seafloor. In addition, the concentration of nitrate in spring and summer is variable, but nitrate usually is sufficient to support some production (see Figs. 2 and 5 in Mordy et al., 2020). With both light and nutrients, the contribution of continued primary production on the seafloor can be substantial and should be considered in estimating primary production in the Chukchi Sea.

4.2. MPL hypothesis

Our results support the hypothesis that continued photosynthesis by disassociated ice algae at the seafloor provides another source of primary production in addition to the spring phytoplankton bloom in the surface mixed layer (Arrigo et al., 2012; Lowry et al., 2014, 2018), the subsurface phytoplankton blooms in the nutrient rich water beneath the surface mixed layer (Lowry et al., 2015; Martini et al., 2016), and the sympagic algal bloom (Gradinger, 2009; Poulin et al., 2011). There is also evidence of a late summer phytoplankton bloom, when summer/fall storms entrain water from the nutrient-rich lower layer (Hill et al., 2017; Ardyna et al., 2014). Together, the various blooms form Multiple Productive Layers that we term the MPL Hypothesis. The MPL hypothesis explains why the Chukchi Sea is highly productive even with a short growing season.

The Chukchi Sea is an inflow shelf (Carmack and Wassmann, 2006). The Arctic Marine Pulses Model describes the Chukchi Sea ecosystem as being dominated by various pulses from the Bering Sea into the Chukchi Sea and from the Arctic basin onto the Chukchi Shelf (Moore et al., 2018). On monthly time scales, inflow through Bering Strait is typically weak in the winter, but in summer this changes with a strong northward flow ($>1 \times 10^6 \text{ m}^3 \text{ s}^{-1}$) of relatively warm nutrient-rich, Bering Sea water into the Chukchi Sea (Coachman et al., 1975; Mordy et al., 2020). With the melting of sea ice, a strong pulse of carbon (e.g. ice algae) is exported to the benthic community—an important pelagic-benthic coupling that supports the rich benthic community of the Chukchi Sea (Grebmeier, 2012; Koch et al., 2020). Herein, we add that while there is a sudden pulse of ice algae to the bottom with sea ice melting; in the Chukchi Sea, this near-bottom water remains productive for weeks to months.

4.3. Comparison of Chukchi and Bering Seas

The relationship between the onset of the growing season and ice retreat for the Chukchi Sea also occurs in the northern Bering Sea, but

not in the southeastern Bering Sea (Sigler et al., 2014). In the southeastern Bering Sea, the timing of the spring bloom (ice algae and phytoplankton) is dependent on ice and winds (Sigler et al., 2014). If ice retreats early (prior to March 15) or is not present at all, storms continue to mix the upper water column, and the spring bloom commences only after surface waters have warmed enough to stratify the vertical structure. This bloom is only composed of phytoplankton. If ice retreat is late, melt water stabilizes the water column and promotes an early spring, under-ice algal bloom, as well as an open-water phytoplankton bloom near the ice edge. The latter pattern is what occurs in the northern Bering Sea, at least until 2018 (Stabeno and Bell, 2019; Stabeno et al., 2019). In 2018, the lack of sea ice in the northern Bering Sea (mooring M8; 62.2°N, 174.7°W) resulted in a late (June) open water bloom, similar to what occurs in the southeastern Bering Sea during years when there is no ice on the southern shelf after 15 March. While subsurface blooms are uncommon in the southeastern Bering Sea, the northern Bering Sea is similar to the Chukchi Sea, with subsurface blooms being common (Stabeno et al., 2012).

The timing of the spring bloom in the southeastern Bering Sea affects the zooplankton species of the ecosystem, a phenomenon described as the Oscillating Control Hypothesis (OCH) (Hunt et al., 2002, 2011; Stabeno and Hunt, 2002). This control likely is spatially determined and related to the location of the ice edge (Siddon et al., 2013; Sigler et al., 2016). The region where the OCH is effective appears to be moving north as climate warms. For example, the entire eastern Bering Sea Shelf was largely ice free in the winter of 2017–2018, a radical change that was not predicted to occur for at least a few decades (Stabeno et al., 2012; Stabeno and Bell, 2019). The lack of ice had widespread effects on the survival of large crustacean zooplankton and juvenile walleye pollock (Duffy-Anderson et al., 2017). Whether and when the OCH region will move into the Chukchi Sea remains to be examined.

Continued productivity of ice algae that has sunk to the seafloor is probably much greater for the Chukchi Sea Shelf than the eastern Bering Sea Shelf, because the latter's bottom depth is mostly below the photic zone. The eastern Bering Sea Shelf deepens from east to west and the mid-shelf is 50–100 m deep whereas the eastern Chukchi Sea Shelf is predominantly shallower than 45 m. Thus, in the Bering Sea, primary production is limited to under-ice algal blooms, surface mixed layer phytoplankton blooms and subsurface phytoplankton blooms, while in the Chukchi Sea, there is evidence of additional disassociated ice algal production near the seafloor.

4.4. What are the consequences of a shorter ice season?

Sea ice in the Chukchi Sea has been arriving later and retreating earlier for ~30 years (Wood et al., 2015; Serreze et al., 2016; Stroeve et al., 2014) and this pattern is expected to continue (Wang et al., 2018). How changes in ice arrival and retreat will impact primary production in the Chukchi ecosystem is dependent upon how other ecosystem characteristics change. Consider two scenarios (from Berchok et al., 2015). As ice retreats earlier, there will be an earlier export of ice algae to the benthos, but the timing of the spring phytoplankton bloom depends upon wind conditions. If winds are strong, then the water column will be well mixed and the spring phytoplankton bloom will not set up until after winds weaken and water becomes stratified. In contrast, if winds are weak the water column will stratify with a warm, fresher (from ice melt) surface layer. This would support an earlier spring phytoplankton bloom. The first scenario will result in weaker stratification than the second scenario, allowing more short summer blooms supported by input of nutrients during wind events. The complexity of the system makes it difficult to predict how this ecosystem will react to changing ice conditions, but there is consensus on some changes.

With climate warming, there will be a decrease in the duration of sea ice over the Chukchi Sea (Wang et al., 2018). Earlier ice retreat will result in earlier export of ice algae to the seafloor, where there should be sufficient nutrients and light to support a near bottom algal bloom

(Tedesco et al., 2019). The one caveat to this scenario is: can the sea-ice retreat occur “too early”. Considering that from our analysis there is insufficient light after the fall equinox to support algal production on the seafloor, it is likely that any ice algae dropping to the seafloor before the spring equinox, also will be non-productive. Ice retreat prior to the spring equinox, however, is not predicted to occur prior to 2050 (Wang et al., 2018). In contrast to earlier ice retreats, delayed ice return will have little impact on near-bottom algal blooms, since they are largely controlled by the availability of light.

Ice algae, however, is only one component in primary production in the Chukchi Sea. Changes in phytoplankton blooms in spring (upper mixed layer), in the summer (sub-pycnocline) and fall (near surface) have been discussed by others. In open water, phytoplankton production may increase, because of a longer growing season (Arrigo and van Dijken, 2015; Arrigo et al., 2008; Brown et al., 2015), although nutrients could be limiting. Once nutrients are consumed in the surface layer, a bloom often forms below the surface mixed layer (e.g. Martini et al., 2016; Lowry et al., 2015). This bloom can be substantial, providing more than a third of primary productivity in the Beaufort Sea (Martin et al., 2013). Churnside et al. (2020) suggest that with reduction in sea ice, the occurrence of these subsurface blooms could increase. These subsurface phytoplankton blooms would likely compete for nutrients with the near-bottom algal blooms and may reduce near-bottom algal production through shading.

5. Summary

The Chukchi Sea is highly productive even though the growing season is short. We provide evidence of production at multiple layers and hypothesize that near-bottom production is a result of disassociated ice algae near the seafloor. On the basis of this evidence, we propose the MPL hypothesis, where high production is promoted by a shallow seafloor, which allows multiple production layers (surface, sub-surface, sympagic ice algae, and disassociated ice algae near the seafloor; Fig. 2). High production occurs because the amount of light near the seafloor in mid-spring to early fall is similar to that measured beneath a 1.5-m thick ice floe. With sufficient light near the seafloor (~40 m deep), ice algae continue to photosynthesize, utilizing nitrate and producing oxygen through summer; a unique feature that pertains to this shallow shelf.

Bloom onset occurred in summer following ice retreat, whereas the end of the bloom occurred in September following loss of light. While this is a complex system, with multiple feedbacks and thus difficult to predict, our results do suggest certain possibilities. Even in a changing system with ice retreating later and arriving earlier, the primary change will be the timing of the export of ice algae to the bottom. Thus, the duration of near-bottom primary productivity will lengthen, because bloom onset occurs earlier.

CRediT authorship contribution statement

Phyllis J. Stabeno: Conceptualization, Methodology, Validation, Resources, Formal analysis, Investigation, Data curation, Writing - original draft, Writing - review & editing, Funding acquisition, Supervision, Visualization. **Calvin W. Mordy:** Conceptualization, Methodology, Validation, Resources, Investigation, Data curation, Funding acquisition, Writing - original draft, Writing - review & editing. **Michael F. Sigler:** Conceptualization, Methodology, Formal analysis, Writing - original draft, Writing - review & editing, Supervision, Visualization.

Declaration of competing interest

The authors declare that they have no known competing financial interests or personal relationships that could have appeared to influence the work reported in this paper.

Acknowledgements

Support was provided by the National Oceanic and Atmospheric Administration; the Bureau of Ocean Energy Management CHAOZ, CHAOZ-X and ArcWEST programs; the NPPR Arctic Program (A92-02a, A92-02b); and the Joint Institute for the Study of the Atmosphere and Ocean (JISAO) under NOAA Cooperative Agreement NA15OAR4320063. We thank S. Bell for data analysis; S. Donohoe for building the pop-up buoys; Leo MacLeod for tracking the ice floe; C. Berchok for being principal investigator on the three BOEM programs, and S. Salo, D. Strausz, G. Lebon, and S. Grassia, for preparing equipment, processing data, and deploying and recovering the moorings. This manuscript is included as part of the North Pacific Research Board (NPPR) Arctic Integrated Ecosystem Research Program, NPPR publication ArcticIERP-09. It is contribution No. 5010 for Pacific Marine Environmental Laboratory, contribution No. 2020-1064 for JISAO, and contribution No. 0933 for NOAA's Ecosystem Fisheries Oceanography Coordinated Investigations.

Appendix A. Supplementary data

Supplementary data to this article can be found online at <https://doi.org/10.1016/j.dsr2.2020.104842>.

References

- Ambrose, W.G., Von Quillfeldt, C., Clough, L.M., Tilney, P.V., Tucker, T., 2005. The sub-ice algal community in the Chukchi sea: large-and small-scale patterns of abundance based on images from a remotely operated vehicle. *Polar Biol.* 28 (10), 784–795.
- Ardyna, M., Babin, M., Gosselin, M., Devred, E., Rainville, L., Tremblay, J.-É., 2014. Recent Arctic Ocean sea ice loss triggers novel fall phytoplankton blooms. *Geophys. Res. Lett.* 41 (17), 6207–6212. <https://doi.org/10.1002/2014GL061047>.
- Arrigo, K.R., van Dijken, G.L., 2011. Secular trends in Arctic Ocean net primary production. *J. Geophys. Res. Oceans* 116(C9), C09011. <https://doi.org/10.1029/2011JC007151>.
- Arrigo, K.R., van Dijken, G., 2015. Continued increases in Arctic Ocean primary production. *Prog. Oceanogr.* 136, 60–70. <https://doi.org/10.1016/j.pocean.2015.05.002>.
- Arrigo, K.R., van Dijken, G., Pabi, S., 2008. Impact of a shrinking Arctic ice cover on marine primary production. *Geophys. Res. Lett.* 35, L19603. <https://doi.org/10.1029/2008GL035028>.
- Arrigo, K.R., Perovich, D., Pickart, R., Brown, Z., van Dijken, G., Lowry, K., et al., 2012. Massive phytoplankton blooms under Arctic sea ice. *Science* 336(6087) 1408. <https://doi.org/10.1126/science.1215065>.
- Berchok, C.L., Crane, J.L., Garland, E.C., Mocklin, J.A., Stabeno, P.J., Napp, J.M., Rone, B.K., Spear, A.H., Wang, M., Clark, C.W., 2015. Chukchi Offshore Monitoring In Drilling Area (COMIDA): Factors Affecting the Distribution and Relative Abundance of Endangered Whales and Other Marine Mammals in the Chukchi Sea. Final Report of the Chukchi Sea Acoustics, Oceanography, and Zooplankton Study, OCS Study BOEM 2015-034. National Marine Mammal Laboratory, Alaska Fisheries Science Center, NMFS, NOAA, 7600 Sand Point Way NE, Seattle, WA 98115-6349.
- Boetius, A., Albrecht, S., Bakker, K., Bienhold, C., Felden, J., Fernández-Méndez, M., Hendricks, S., Katlein, C., Lalander, C., Krumpen, T., Nicolais, M., 2013. Export of algal biomass from the melting Arctic sea ice. *Science* 339 (6126), 1430–1432.
- Brown, Z.W., Lowry, K.E., Palmer, M.A., van Dijken, G.L., Mills, M.M., Pickart, R.S., Arrigo, K.R., 2015. Characterizing the subsurface chlorophyll *a* maximum in the Chukchi sea and Canada basin. *Deep-Sea Res. Part II* 118 (A), 88–104. <https://doi.org/10.1016/j.dsr2.2015.02.010>.
- Carmack, E., Wassmann, P., 2006. Food webs and physical-biological coupling on pan-Arctic shelves: unifying concepts and comprehensive perspectives. *Prog. Oceanogr.* 71, 446–477.
- Castellani, G., Losch, M., Lange, B., Flores, H., 2017. Modeling Arctic sea-ice algae: physical drivers of spatial distribution and algae phenology. *J. Geophys. Res. Oceans* 122, 7466–7487. <https://doi.org/10.1002/2017JC012828>.
- Churnside, J.H., Marchbanks, R.D., Vagle, S., Bell, S.W., Stabeno, P.J., 2020. Stratification, plankton layers, and mixing measured by airborne lidar in the Chukchi and Beaufort seas. *Deep-Sea Res. Part II* this issue.
- Coachman, L.K., Aagaard, K., Tripp, R.B., 1975. Bering Strait: The Regional Physical Oceanography. University of Washington Press, Seattle, WA.
- Codispoti, L.A., Kelly, V., Thessen, A., Matrai, P., Suttles, S., Hill, V., Steele, M., Light, B., 2013. Synthesis of primary production in the Arctic Ocean: III. Nitrate and phosphate based estimates of net community production. *Prog. Oceanogr.* 110, 126–150.
- Cota, G.F., Horne, E.P.W., 1989. Physical control of arctic ice algal production. *Mar. Ecol. Prog. Ser.* 52, 111–121.
- Cota, G.F., Prinsenberg, S.J., Bennett, E.B., Loder, J.W., Lewis, M.R., Anning, J.L., et al., 1987. Nutrient fluxes during extended blooms of Arctic ice algae. *J. Geophys. Res.: Oceans* 92 (C2), 1951–1962.

- Danielson, S.L., Ahkinga, O., Ashjian, C., Basuk, E., Cooper, L.W., Eisner, L., et al., 2020. Manifestation and consequences of warming and altered heat fluxes over the Bering and Chukchi Sea continental shelves. *Deep-Sea Res. Part II* this issue.
- Duffy-Anderson, J.T., Stabeno, P.J., Siddon, E.C., Andrews, A.G., Cooper, D.W., Eisner, L.B., Farley, E.V., Harpold, C.E., Heintz, R.A., Kimmel, D.G., Sewall, F.F., Spear, A.H., Yasumishii, E.C., 2017. Return of warm conditions in the southeastern Bering Sea: phytoplankton-fish. *PLoS ONE* 12(6), e0178955. <https://doi.org/10.1371/journal.pone.0178955>.
- Dunton, K.H., Grebmeier, J.M., Trefry, J.H., 2014. The benthic ecosystem of the northeastern Chukchi Sea: an overview of its unique biogeochemical and biological characteristics. *Deep-Sea Res. Part II* 102, 1–8. <https://doi.org/10.1016/j.dsr2.2014.01.001>.
- Fernández-Méndez, M., Wenzhöfer, F., Peeken, I., Sørensen, H.L., Glud, R.N., Boetius, A., 2014. Composition, buoyancy regulation and fate of ice algal aggregates in the Central Arctic Ocean. *PLoS One* 9 (9), e107452. <https://doi.org/10.1371/journal.pone.0107452>.
- Frey, K.E., Moore, G.W.K., Cooper, L.W., Grebmeier, J.M., 2015. Divergent patterns of recent sea ice cover across the bering, Chukchi, and Beaufort seas of the pacific arctic region. *Prog. Oceanography* 136, 32–49.
- Gradinger, R., 2009. Sea-ice algae: major contributors to primary production and algal biomass in the Chukchi and Beaufort Seas during. *Deep-Sea Res. Part II* 56 (17), 1201–1212. <https://doi.org/10.1016/j.dsr2.2008.10.016>. May/June 2002.
- Grebmeier, J., 2012. Shifting patterns of life in the Pacific Arctic and sub-arctic seas. *Annu. Rev. Mar. Sci.* 4, 1–16.
- Grebmeier, J., Overland, J.E., Moore, S.E., Farley, E.V., Carmack, E.C., Cooper, L.W., Frey, K.E., Helle, J.H., McLaughlin, F.A., McNutt, S.L., 2006. A major ecosystem shift in the northern Bering Sea. *Science* 311, 1461–1464. <https://doi.org/10.1126/science.1121365>.
- Grebmeier, J., Bluhm, B., Cooper, L., Denisenko, S., Iken, K., Kedra, M., Serratos, C., 2015. Time-series benthic community composition and biomass and associated environmental characteristics in the Chukchi Sea during the RUSALCA 2004–2012 program. *Oceanography* 28 (3), 116–133.
- Hancke, K., Lund-Hansen, L.C., Lamare, M.L., Højlund Pedersen, S., King, M.D., Andersen, P., Sorrell, B.K., 2018. Extreme low light requirement for algae growth underneath sea ice: a case study from Station Nord, NE Greenland. *J. Geophys. Res. Oceans* 123, 985–1000. <https://doi.org/10.1002/2017JC013263>.
- Hill, V., Cota, G., 2005. Spatial patterns of primary production on the shelf, slope and basin of the Western Arctic in 2002. *Deep-Sea Res. Part II* 52 (24–26), 3344–3354.
- Hill, V., Ardyna, M., Lee, S., Varela, D., 2017. Decadal trends in phytoplankton production in the Pacific Arctic region from 1950 to 2012. *Deep-Sea Res. Part II* 152, 82–94. <https://doi.org/10.1016/j.dsr2.2016.12.015>.
- Hirano, D., Fukamachi, Y., Watanabe, E., Ohshima, K.I., Iwamoto, K., Mahoney, A.R., Eicken, H., Simizu, D., Tamura, T., 2016. A wind-driven, hybrid latent and sensible heat coastal polynya off Barrow, Alaska. *J. Geophys. Res. Oceans* 121, 980–997. <https://doi.org/10.1002/2015JC011318>.
- Hunt Jr., G.L., Stabeno, P., Walters, G., Sinclair, E., Brodeur, R.D., Napp, J.M., Bond, N.A., 2002. Climate change and control of the southeastern Bering Sea pelagic ecosystem. *Deep-Sea Res. Part II* 49 (26), 5821–5853. [https://doi.org/10.1016/S0967-0645\(02\)00321-1](https://doi.org/10.1016/S0967-0645(02)00321-1).
- Hunt Jr., G.L., Coyle, K.O., Eisner, L., Farley, E.V., Heintz, R., Mueter, F., Napp, J.M., Overland, J.E., Ressler, P.H., Salo, S., Stabeno, P.J., 2011. Climate impacts on eastern Bering Sea foodwebs: a synthesis of new data and an assessment of the Oscillating Control Hypothesis. *ICES J. Mar. Sci.* 68 (6), 1230–1243. <https://doi.org/10.1093/icesjms/fsr036>.
- Katlein, C., Fernández-Méndez, M., Wenzhöfer, F., Nicolaus, M., 2015. Distribution of algal aggregates under summer sea ice in the Central Arctic. *Polar Biol.* 38 (5), 719–731.
- Koch, C.W., Cooper, L.W., Lalande, C., Brown, T.A., Frey, K.E., Grebmeier, J.M., 2020. Seasonal and latitudinal variations in sea ice algal deposition in the Northern Bering and Chukchi Seas determined by algal biomarkers. *PLoS ONE* 15(4), e0231178. <https://doi.org/10.1371/journal.pone.0231178>.
- Ladd, C., Mordy, C.W., Salo, S.A., Stabeno, P.J., 2016. Winter water properties and the Chukchi polynya. *J. Geophys. Res.* 121 (8), 5516–5534. <https://doi.org/10.1002/2016JC011918>.
- Langis, D., Stabeno, P.J., Meinig, C., Mordy, C.W., Bell, S.W., Tabisola, H.M., October 2018. Low-cost expendable buoys for under ice data collection. In: Oceans 2018 MTS/IEEE Charleston, Marine Technology Society and IEEE Oceanic Engineering Society. IEEE, Charleston, SC, pp. 22–25. <https://doi.org/10.1109/OCEANS.2018.8604752>.
- Lowry, K.E., van Dijken, G.L., Arrigo, K.R., 2014. Evidence of under-ice phytoplankton blooms in the Chukchi sea from 1998 to 2012. *Deep Sea Res. Part II* 105, 105–117. <https://doi.org/10.1016/j.dsr2.2014.03.013>.
- Lowry, K.E., Pickart, R.S., Mills, M.M., Brown, Z.W., van Dijken, G.L., Bates, N.R., Arrigo, K.R., 2015. The influence of winter water on phytoplankton blooms in the Chukchi Sea. *Deep-Sea Res. Part II* 118, 53–72.
- Lowry, K.E., Pickart, R.S., Selz, V., Mills, M.M., Pacini, A., Lewis, K.M., et al., 2018. Under-ice phytoplankton blooms inhibited by spring convective mixing in refreezing leads. *J. Geophys. Res. Oceans* 123 (1), 90–109.
- Martin, J., Dumont, D., Tremblay, J.-É., 2013. Contribution of subsurface chlorophyll maxima to primary production in the coastal Beaufort Sea (Canadian Arctic): a model assessment. *J. Geophys. Res. Oceans* 118 (11), 5873–5886. <https://doi.org/10.1002/2013JC008843>.
- Martini, K.I., Stabeno, P.J., Ladd, C., Winsor, P., Weingartner, T.J., Mordy, C.W., Eisner, L.B., 2016. Dependence of subsurface chlorophyll on seasonal water masses in the Chukchi Sea. *J. Geophys. Res.* 121 (3), 1755–1770. <https://doi.org/10.1002/2015JC011359>.
- Michel, C., Legendre, L., Demers, S., Therriault, J.-C., 1988. Photoadaptation of sea-ice microalgae in springtime: photosynthesis and carboxylating enzymes. *Mar. Eco. Prog. Ser.* 50, 177–185.
- Michel, C., Legendre, L., Therriault, J.-C., Demers, S., Vandavelde, T., 1993. Springtime coupling between ice algal and phytoplankton assemblages in southeastern Hudson Bay, Canadian Arctic. *Polar Biol.* 13, 441–449. <https://doi.org/10.1007/BF00233135>.
- Moore, S.E., Stabeno, P.J., 2015. Synthesis of arctic Research (SOAR) in marine ecosystems of the pacific arctic. *Prog. Oceanography* 136, 1–11. <https://doi.org/10.1016/j.pocean.2015.05.017>.
- Moore, S.E., Stabeno, P.J., Grebmeier, J.M., Okkonen, S.R., 2018. The arctic marine pulses model: linking annual oceanographic processes to contiguous ecological domains in the pacific arctic. *Deep-sea res. Part II* 152. SOAR II 8–21. <https://doi.org/10.1016/j.dsr2.2016.10.011>.
- Mordy, C., Bell, S., Cokelet, E., Ladd, C., Lebon, G., Proctor, P., Stabeno, P., Strausz, D., Wisegarver, E., 2020. This Issue. Seasonal Variability of Nitrate in the Eastern Chukchi Sea. *Deep-Sea Res. Part II*.
- Neeley, A.R., Harris, L.A., Frey, K.E., 2018. Unraveling phytoplankton community dynamics in the northern Chukchi Sea under sea-ice-covered and sea-ice-free conditions. *Geophys. Res. Lett.* 45 (15), 7663–7671.
- Poulin, M., Daugbjerg, N., Gradinger, R., Ilyash, L., Ratkova, T., von Quillfeldt, C., 2011. The pan-Arctic biodiversity of marine pelagic and sea-ice unicellular eukaryotes: a first-attempt assessment. *Mar. Biodivers.* 41, 13–28. <https://doi.org/10.1007/s12526-010-0058-8>.
- Rapp, J.Z., Fernández-Méndez, M., Bienhold, C., Boetius, A., 2018. Effects of ice-algal aggregate export on the connectivity of bacterial communities in the central Arctic Ocean. *Front. Microbiol.* 9, 1035.
- Riebesell, U., Schloss, I., Smetacek, V., 1991. Aggregation of algae released from melting sea ice: implications for seeding and sedimentation. *Polar Biol.* 11 (4), 239–248.
- Serreze, M.C., Crawford, A.D., Stroeve, J.C., Barrett, A.P., Woodgate, R.A., 2016. Variability, trends, and predictability of seasonal sea ice retreat and advance in the Chukchi Sea. *J. Geophys. Res. Oceans* 121 (10), 7308–7325. [https://doi.org/10.1002/2016jc011977](https://doi.org/10.1002/10.1002/2016jc011977).
- Siddon, E., Heintz, R., Mueter, F., 2013. Conceptual model of energy allocation in walleye pollock (*Theragra chalcogramma*) from age-0 to age-1 in the southeastern Bering Sea. *Deep-Sea Res. Part II* 94, 140–149. <https://doi.org/10.1016/j.dsr2.2012.12.007>.
- Sigler, M.F., Stabeno, P.J., Eisner, L.B., Napp, J.M., Mueter, F.J., 2014. Spring and fall phytoplankton blooms in a productive subarctic ecosystem, the eastern Bering Sea, during 1995–2011. *Deep-Sea Res. Part II* 109, 71–83. <https://doi.org/10.1016/j.dsr2.2013.12.007>.
- Sigler, M.F., Napp, J.M., Stabeno, P.J., Heintz, R.A., Lomas, M.W., Hunt Jr., G.L., 2016. Variation in annual production of copepods, euphausiids, and juvenile walleye pollock in the southeastern Bering Sea. *Deep-Sea Res. Part II* 134, Understanding Ecosystem Processes in the Eastern Bering Sea IV 223–234. <https://doi.org/10.1016/j.dsr2.2016.01.003>.
- Stabeno, P.J., Bell, S.W., 2019. Extreme conditions in the Bering Sea (2017–2018): record-breaking low sea-ice extent. *Geophys. Res. Lett.* 46 (15), 8952–8959. <https://doi.org/10.1029/2019GL083816>.
- Stabeno, P.J., Hunt Jr., G.L., 2002. Overview of the inner front and southeast Bering Sea carrying capacity programs. *Deep-Sea Res. Part II* 49 (26), 6157–6168. [https://doi.org/10.1016/S0967-0645\(02\)00339-9](https://doi.org/10.1016/S0967-0645(02)00339-9).
- Stabeno, P.J., Farley, E., Kachel, N., Moore, S., Mordy, C., Napp, J.M., Overland, J.E., Pinchuk, A.I., Sigler, M.F., 2012. A comparison of the physics of the northern and southern shelves of the eastern Bering Sea and some implications for the ecosystem. *Deep-Sea Res. Part II* 65–70, 14–30. <https://doi.org/10.1016/j.dsr2.2012.02.019>.
- Stabeno, P., Kachel, N., Ladd, C., Woodgate, R., 2018. Flow patterns in the eastern Chukchi sea: 2010–2015. *J. Geophys. Res.* 123 (2), 1177–1195. <https://doi.org/10.1002/2017JC013135>.
- Stabeno, P.J., Bell, S., Bond, N., Kimmel, D., Mordy, C., Sullivan, M., 2019. Distributed biological observatory region 1: physics, chemistry and plankton in the northern Bering Sea. *Deep-Sea Res. Part II* 162, 8–21. <https://doi.org/10.1016/j.dsr2.2018.11.006>.
- Stroeve, J.C., Markus, T., Boisvert, L., Miller, J., Barret, A., 2014. Changes in Arctic melt season and implications for sea ice loss. *Geophys. Res. Lett.* 41, 1216–1225. <https://doi.org/10.1002/2013GL058951>.
- Tedesco, L., Vichi, M., Scoccimarro, E., 2019. Sea-ice algal phenology in a warmer Arctic. *Sci. Adv.* 5 (5), eaav4830. <https://doi.org/10.1126/sciadv.aav4830>.
- Tremblay, G., Belzile, C., Gosselin, M., Poulin, M., Roy, S., Tremblay, J.-É., 2009. Late summer phytoplankton distribution along a 3500 km transect in Canadian Arctic waters: strong numerical dominance by picoeukaryotes. *Aquat. Microb. Ecol.* 54 (1), 55–70.
- Wang, M., Yang, Q., Overland, J.E., Stabeno, P.J., 2018. Sea-ice cover timing in the Pacific Arctic: the present and projections to mid-century by selected CMIP5 models. *Deep-Sea Res. Part II* 152. SOAR II 22–34. <https://doi.org/10.1016/j.dsr2.2017.11.017>.
- Welch, H.E., Bergmann, M.A., 1989. Seasonal development of ice algae and its prediction from environmental factors near Resolute, NWT, Canada. *Can. J. Fish. Aquat. Sci.* 46 (10), 1793–1804.
- Wood, K.R., Bond, N.A., Overland, J.E., Salo, S.A., Stabeno, P., Whitefield, J., 2015. A decade of environmental change in the Pacific Arctic region. *Prog. Oceanography* 136, 12–31. <https://doi.org/10.1016/j.pocean.2015.05.005>.
- Wood, K.R., Jayne, S.R., Mordy, C.W., Bond, N., Overland, J.E., Ladd, C., Stabeno, P.J., Ekholm, A.K., Robbins, P.E., Schreck, M.-B., Heim, R., Intrieri, J., 2018. Results of the first Arctic Heat Open Science Experiment. *Bull. Am. Meteorol. Soc.* 99 (3), 513–520. <https://doi.org/10.1175/BAMS-D-16-0323.1>.